Estimation of above- and below-ground ecosystem parameters for the DVM-DOS-TEM v0.7.0 model using MADS v1.7.3

Elchin E. Jafarov[1], Hélène Genet[2], Velimir V. Vesselinov (Monty)[3], Valeria Briones[1], Aiza Kabeer[4], Andrew L. Mullen[1], Benjamin Maglio[2], Tobey Carman[2], Ruth Rutter[2], Joy Clein[2], Chu-Chun Chang[1], Dogukan Teber[1], Trevor Smith[1], Joshua M. Rady[1], Christina Schädel[1], Jennifer D. Watts[1], Brendan M. Rogers[1], Susan M. Natali[1]

[1]Woodwell Climate Research Center, Falmouth, MA, USA
[2]Institute of Arctic Biology, University of Alaska Fairbanks, Fairbanks, AK, USA
[3]EnviTrace LLC, NM, USA
[4]Program in Applied Mathematics, University of Arizona, Tucson, AZ, USA

Correspondence to: Elchin E. Jafarov (ejafarov@woodwellclimate.org)

Abstract.
The permafrost region contains a significant portion of the world's soil organic carbon, and its thawing, driven by accelerated Arctic warming, could lead to the substantial release of greenhouse gases, potentially disrupting the global climate system. Accurate predictions of carbon cycling in permafrost ecosystems hinge on the robust calibration of model parameters. However, manually calibrating numerous parameters in complex process-based models is labor-intensive and further complicated by equifinality - the presence of multiple parameter sets that can equally fit the observed data. Incorrect calibration can lead to unrealistic ecological predictions. In this study, we employed the Model Analysis and Decision Support (MADS) software package to automate and enhance the accuracy of parameter calibration for carbon dynamics within the coupled Dynamic Vegetation Model, Dynamic Organic Soil Model, and Terrestrial Ecosystem Model (DVM-DOS-TEM), a process-based ecosystem model designed for high-latitude regions. The calibration process involved adjusting rate-limiting parameters to accurately replicate observed carbon and nitrogen fluxes and stocks in both soil and vegetation. Gross primary production, net primary production, vegetation carbon, vegetation nitrogen, and soil carbon and nitrogen pools served as synthetic observations for a black spruce boreal forest ecosystem. To validate the efficiency of this new calibration method, we utilized model-generated synthetic and actual observations. When matching model outputs to observed data, we encountered difficulties in maintaining mineral soil carbon stocks. Additionally, due to strong interdependencies between parameters and target values, the model consistently overestimated carbon and nitrogen allocation to the stem of evergreen tree. This study demonstrates the calibration workflow, offers an in-depth analysis of the relationships between parameters and observations (synthetic and actual), and evaluates the accuracy of the calibrated parameter values.

1 Introduction

The permafrost region contains 1,440-1,600 petagrams of organic carbon in its soils, representing nearly half of the world's soil organic carbon pool (Hugelius et al., 2014; Schuur et al., 2022). Accelerated warming in the Arctic leads to permafrost thaw, resulting in the decomposition and potential release of a substantial portion of this stored carbon as greenhouse gases, significantly impacting the global climate system (Natali et al., 2021; Schuur et al., 2022; Treharne et al., 2022). The permafrost carbon-climate feedback remains one of the largest sources of model uncertainty for future climate predictions, as critical ecological and biogeochemical processes are poorly represented and constrained in ecosystem models, if included at all (McGuire et al., 2016, 2018; Schädel et al., 2024). A significant portion of this uncertainty stems from parameter uncertainty, particularly in rate-limiting factors that control biogeochemical cycles, which are challenging to measure directly and can vary considerably across spatial and temporal scales (Koven et al., 2015; Mishra et al., 2021). These uncertainties propagate through model simulations, contributing to a wide range of projected permafrost carbon emissions (Lawrence et al., 2015; McGuire et al., 2018).

When compared to structural uncertainty (which arises from incomplete or simplified representations of ecological processes) and input data uncertainty (resulting from limited or biased forcing datasets), parameter uncertainty is particularly pervasive and difficult to constrain (Euskirchen et al., 2022; Fisher and Koven, 2020; Luo et al., 2016). While structural uncertainties limit a model's ability to fully capture real-world processes, parameter uncertainties directly alter numerical outputs, often amplifying variations in projections (Fisher and Koven, 2020; Turetsky et al., 2020). Models are particularly sensitive to parameter uncertainties, given the complexity and variability of the processes they simulate, including soil thermal dynamics, vegetation feedbacks, and hydrological interactions (Andresen et al., 2020; Harp et al., 2016; Koven et al., 2015). While structural improvements to model frameworks are ongoing, addressing parameter uncertainty through robust calibration methods remains an essential and complementary step for enhancing the accuracy and reliability of model outputs (Fisher and Koven, 2020; Luo et al., 2016). Addressing these uncertainties through the development of effective calibration techniques is essential for refining predictions of permafrost dynamics and better constraining future permafrost carbon-climate feedbacks (McGuire et al., 2018; Mishra et al., 2021).

Calibration involves estimating and adjusting model parameters to enhance the agreement between model outputs and observed data, with the model serving as a mathematical representation of ecological and physical processes (Rykiel, 1996). These parameters are often rate or transport constants that are onerous or impractical to empirically estimate, though model outputs can be highly sensitive to them. Since many model representations are grounded in physics, generalized physical laws are often used to describe ecological and cryohydrological processes. Typically, model outputs are validated against data from laboratory experiments, idealized mathematical models, or site-specific observations, also referred to as target data. During this validation, model parameters are adjusted so that model outputs match the target data. The validated model is then applied to broader geographic locations and/or different time periods, assuming that the validation data represent the environment or ecosystem for which the parameters were calibrated.

Parameter calibration for complex process-based models is often constrained by the significant labor required and the limited availability of sites with the necessary observations, especially in permafrost regions (Birch et al., 2021; Virkkala et al., 2019). Despite these challenges, process-based models remain essential because they encapsulate our current understanding of ecosystem functions and structures, serving as powerful tools for extrapolation. The assumption of representativeness is intrinsic to these models, as they are designed to simulate processes that reflect our best understanding of ecosystem dynamics, allowing for their application beyond the individual sites where they have been initially parameterized. The approach of extrapolating model parameterization for ecosystems of the same type, across wider regions is standard and widely used within ecosystem modeling communities (Matthes et al., 2025; McGuire et al., 2018). Additionally, the role of ecosystem diversity on the spatio-temporal patterns of ecosystem carbon dynamics in the permafrost region has been characterized by numerous empirical studies (Euskirchen et al., 2014; Melvin et al., 2015) and evaluated by modeling investigations (Lara et al., 2016). Therefore, a critical step in improving model accuracy involves calibrating the model against a suite of data for a representative diversity of ecosystem types in the Arctic where observations are available. To prepare an ecosystem model for this extensive calibration task, it is essential to develop robust calibration tools and methods that can automate the process of efficiently optimizing model parameters.

Another well-known and significant issue in optimizing model parameters through calibration, also referred to as parameter estimation or optimization, is the existence of equifinality (Jafarov et al., 2020; Nicolsky et al., 2007; Tran et al., 2017). Parameterization equifinality occurs when different sets of parameter values result in the same or similar model predictions, given that the model, forcing data, and observations used in calibration are the same (Beven and Freer, 2001). Model equifinality can subsequently lead to different outcomes in model projections. In an aim to address the issue of equifinality, we run the model using randomly varied parameter values within the given range. If the majority of calibration tests with different initial guesses yield a good fit with observations and result in optimal parameter sets that are similar or closely aligned, it increases confidence that the recovered parameter set is indeed optimal. This approach mitigates the risk of converging on a local minimum and ensures a more robust and reliable parameter estimation process (Hansen, 1998).

Various methods have been employed to improve the calibration of model parameters across multiple scientific disciplines, utilizing sophisticated techniques and integrating diverse data sources such as remote sensing and field measurements, while accounting for model and data uncertainty (Dietze et al., 2018; Efstratiadis and Koutsoyiannis, 2010; Luo et al., 2016). Optimization-based inverse methods have been successfully used to calibrate parameters in physical models, including snow properties and subsurface thermo-hydrological properties (Jafarov et al., 2014, 2020), as well as soil properties for permafrost modeling (Nicolsky et al., 2007, 2009). However, inverse modeling can become computationally intractable when applied to complex process-based models (Linde et al., 2015).

Markov Chain Monte Carlo (MCMC) and data assimilation (DA) techniques have been employed to optimize model parameters by synchronizing model outputs with observed data, thereby enhancing model prediction accuracy (Brunetti et al., 2023; Fer et al., 2018; Xu et al., 2017). These methods often

leverage Bayesian inference to address structural uncertainties within models. Nonetheless, the computational demand required for conducting MCMC simulations can outweigh the gains in model accuracy, particularly when dealing with complex process-based models with slow turnover rates that necessitate long simulations to reach equilibrium.

In recent years, DA techniques have been applied to optimize both model state variables (Fox et al., 2018; Ling et al., 2019) and parameters (Bloom et al., 2016; Peylin et al., 2016; Scholze et al., 2016; Schürmann et al., 2016). However, DA also encounters challenges related to unbalanced outputs and the need for extended simulations to achieve equilibrium. Persistent issues include the incorrect characterization of the error covariance matrix, which can lead to inaccurate posterior parameter values due to unaccounted model structural errors and observation biases (MacBean et al., 2016; Wutzler and Carvalhais, 2014).

Various surrogate-based optimization approaches have been proposed to alleviate the computational burden associated with parameter calibration (Koziel et al., 2011; Queipo et al., 2005). Surrogate models, also known as reduced-order models, simplify certain physical processes to approximate the underlying dynamics of the real model while being computationally less demanding (Forrester et al., 2006). By simplifying specific aspects of the model, surrogate models retain essential characteristics of the original system, allowing for faster and more efficient calibration without significantly compromising accuracy (Razavi et al., 2012; Regis and Shoemaker, 2007). However, simplifying complex models presents significant challenges. It is often unclear which assumptions can be safely made and which should be avoided, potentially leading to a loss of model accuracy. Surrogate models must carefully balance the trade-off between simplification and the retention of critical model characteristics to ensure reliable performance. This complexity necessitates rigorous validation to confirm that the surrogate model provides an adequate approximation of the real system without introducing significant errors.

In recent years, machine learning-based emulators, often referred to as "models of models," have emerged as a promising approach to reduce the computational burden associated with parameter calibration in complex ecosystem models (Castelletti et al., 2012; Fer et al., 2018; Reichstein et al., 2019). These emulators aim to approximate the outputs of physical and process-based models by learning the relationships between model inputs and outputs through multi-dimensional matrices, significantly enhancing computational efficiency. Unlike traditional surrogate models, which simplify the physical processes within a model, emulators strive to mimic the full complexity of the original model while requiring less computational power. For instance, Dagon et al., (2020) utilized artificial neural networks to emulate the Community Land Model version 5 outputs, focusing on biophysical parameter estimation and global calibration. By integrating machine learning techniques, they were able to explore parameter spaces more efficiently and achieve better alignment with observed data. This method demonstrates the potential of machine learning emulators in improving the accuracy and efficiency of parameter calibration in ecosystem models, particularly when faced with the challenge of high computational demands.

To facilitate the automation of the calibration process while minimizing computational demand and avoiding the oversimplification of ecological processes and feedbacks, we employed a non-linear least squares approach for our calibration. We utilized the Model Analysis and Decision Support (MADS) software package (Barajas-Solano et al., 2015; O'Malley and Vesselinov, 2015) for parameter calibration of a terrestrial ecosystem permafrost-enabled model. MADS has been actively developed since 2010, and its conversion to the Julia programming language has provided automatic differentiation capabilities suitable for calibration problems, improving computational efficiency (Vesselinov V.V., 2022).

In this study, we developed an automated parameter calibration method for a process-based terrestrial ecosystem model developed for high-latitude regions and characterized by a high level of complexity. To demonstrate its efficacy, we utilized synthetic data and evaluated the capacity of the calibration method to recover the data after perturbing initial guesses (a given set of parameters) using random sampling. The model was run using known parameter values, and the resulting outputs were treated as observations. The primary objective was to illustrate that the parameter calibration method could recover the synthetic parameter set successfully. The secondary objective was to optimize and reduce the labor and time associated with manual parameter calibration. We developed and tested our calibration method for the coupled dynamic vegetation model, dynamic organic soil, and terrestrial ecosystem model (DVM-DOS-TEM) and tested our approach using synthetic and site observations at a black spruce forest site, a dominant community type in Interior Alaska.

2 Methods

2.1 Black Spruce Forest site

Approximately 39% of Interior Alaska is covered by evergreen forest stands, dominated by white or black spruce and 24% by deciduous forest stands, dominated by Alaska paper birch or trembling aspen (Calef et al., 2005; Jean et al., 2020). In our study, we developed model calibration for a black spruce (*Picea mariana*) forest community type, using observations collected in a site located within the Tanana Valley State Forest, just outside Fairbanks, Alaska (64°53′N, 148°23′W). Carbon (C) and nitrogen (N) cycling and environmental monitoring in this forest stand were originally observed by Melvin et al., (2015). The stand resulted from a self-replacement succession trajectory following the 1958 Murphy Dome fire, which covered 8,930 hectares.

2.2 DVM-DOS-TEM description

DVM-DOS-TEM is a process-based biosphere model designed to simulate biophysical and biogeochemical processes between the soil, vegetation, and atmosphere. DVM-DOS-TEM has been applied extensively in Arctic and Boreal ecosystems in permafrost and non-permafrost regions (Briones et al., 2024; Euskirchen et al., 2022; Genet et al., 2013, 2018; Jafarov et al., 2013; Yi et al., 2009, 2010). This model focuses on representing C and N cycles in high-latitude ecosystems and how they are affected at seasonal (i.e., monthly) to centennial scales by climate, disturbances (Genet et al., 2013,

188 2018; Kelly et al., 2013), biophysical processes such as soil thermal and hydrological dynamics
189 (McGuire et al., 2018; Yi et al., 2009; Zhuang et al., 2002), snow cover (Euskirchen et al., 2006), and
190 plant canopy development (Euskirchen et al., 2014). Modeled vegetation is structured into multiple
191 tiers: (1) the community type (CMT) represents the land cover class and characterizes vegetation
192 composition and soil structure at the gridcell level (spatial unit, e.g. black spruce forest, tussock tundra,
193 bog), (2) plant functional types (groups of species sharing similar functional traits) characterize the
194 vegetation composition within every CMT (e.g. black spruce forest community would be composed of
195 evergreen trees, deciduous shrubs and sphagnum and feather moss plant functional types), and (3) plant
196 structural compartments (leaves, stems, roots). The soil column is split into multiple horizons (fibric,
197 humic, mineral, and rock/parent material). Every horizon is split into multiple layers for which C, N,
198 temperature, and water content are simulated individually. The biophysical processes represented in
199 DVM-DOS-TEM include radiation and water fluxes between the atmosphere, vegetation, snow cover,
200 and soil column. Soil moisture and temperature are updated at a pseudo-daily time step (from linear
201 interpolation of monthly climate forcings). A two-directional Stefan Algorithm is used to predict the
202 positions of freezing/thawing fronts in the soil. The Richards equation is used to calculate soil moisture
203 changes in the unfrozen layers of soil. Both the thermal and hydraulic properties of soil layers are
204 affected by their water content (Yi et al., 2009, 2010; Zhuang et al., 2002). The ecological processes
205 represented in DVM-DOS-TEM include C and N dynamics for every plant functional type (PFT) of the
206 vegetation community and every layer of the soil column. C and N dynamics are driven by climate,
207 atmospheric CO_2 content, soil and canopy environment, and wildfire occurrence and severity. C and N
208 cycles are coupled in the soil and the vegetation processes. The growth primary productivity (GPP) of
209 each PFT is limited by N availability. When resources in N are limited, GPP is downregulated for all
210 PFTs based on a comparison of N demand (N required to build new tissues) and N supply in the
211 ecosystem (Euskirchen et al., 2009). C and N from the litterfall are divided into aboveground and
212 belowground. Aboveground litterfall is assigned only to the top layer of the soil column, while
213 belowground litterfall (root mortality) is assigned to different layers of the three soil horizons based on
214 the fractional distribution of fine roots with depth.
215
216 **2.3 Synthetic data**
217 We used GPP without N limitation (GPP*), Net Primary Productivity (NPP), Vegetation C, and
218 Vegetation N stocks by compartments (i.e. roots, stems, and leaves) as synthetic observations shown in
219 Table 1. Synthetic observations are model-generated data that simulate actual measurements using
220 known parameter values, referred to as synthetic target values. To generate these target values, we used
221 existing parameters and the setup described in Section 2.3. The target values shown in Table 1 represent
222 the state of the ecosystem where vegetation and below-ground C stocks are in a steady state. Table 2
223 includes the below-ground target values. The model was previously manually calibrated using
224 observations from the site. The actual observations were collected and prepared from the measured data
225 at the site and from existing literature and published datasets. Data pre-processing was required before
226 the time series data could be analyzed. Pre-processing was performed to identify and resolve missing
227 data, inconsistencies, and potential outliers. In addition, site observations were aggregated to a monthly
228 resolution to match the temporal resolution of the model outputs, and unit transformations were applied
229 when needed to standardize the units of each variable. Target values for the site were compiled from

230 various data literature sources containing information on C and N stocks, plant biomass, soil horizon
231 depths, and productivity. However, following the initial calibration, the model outputs were similar but
232 did not exactly match the target observations. As stated above, we choose synthetic targets because we
233 know a set of parameters used to produce them and can compare how closely we can recover known
234 parameter values. Therefore, we used the actual model output as our synthetic target values.

235 **Table 1**: Synthetic vegetation target values for the black spruce forest site used in the parameter
236 calibration process

Above-ground Target Names	Notation	Units	Plant Functional Types			
			Evergreen Tree	Deciduous Shrub	Deciduous Tree	Moss
Gross Primary Productivity without nitrogen limitation	GPP^*	[gC/m²/year]	307.17	24.53	46.53	54.23
Net Primary Productivity	NPP	[gC/m²/year]	113.08	11.3	24.02	32.41
Vegetation Carbon Leaf	C_{leaf}	[gC/m²]	572.36	8.35	6.14	136.54
Vegetation Carbon Stem	C_{stem}	[gC/m²]	1894.03	98.90	477.80	
Vegetation Carbon Root	C_{root}	[gC/m²]	474.55	33.19	7.17	
Vegetation Nitrogen Leaf	N_{leaf}	[gC/m²]	14.79	0.38	0.57	1.15
Vegetation Nitrogen Stem	N_{stem}	[gC/m²]	30.26	2.6	12.53	
Vegetation Nitrogen Root	N_{root}	[gC/m²]	9.51	0.72	0.16	

237
238
239 **Table 2**: Synthetic below-ground target values for the black spruce forest site used in the parameter
240 calibration process

Below-ground Targets Names	Notation	Unit	Value
Carbon Shallow	$C_{shallow}$	g/m2	888.91

Carbon Deep	C_{deep}	g/m2	3174.53
Carbon Mineral Sum	$\sum C_{mineral}$	g/m2	19821.50
Available Nitrogen Sum	$\sum N_{avail}$	g/m2	0.76

241

2.4 Input data used for equilibrium run

243 The driving inputs for the DVM-DOS-TEM model comprise spatial distribution of CMTs, landform,
244 and mineral soil texture. These initialization data were forced to field observations at the study site
245 (Melvin et al., 2015). The spatiotemporal dynamics of the model are driven by an annual time series of
246 atmospheric CO_2 concentration (not spatially explicit), annual time series of spatially explicit
247 distribution of fire scars and dates, and a spatially explicit monthly time series of climate, including
248 mean air temperature, total precipitation, net incoming shortwave radiation, and vapor pressure (Genet
249 et al., 2018). For the present study, we use historical climate data from 1901 to 2015, sourced from the
250 Climatic Research Unit time series version 4.0 (CRU TS4.0; Harris et al., 2014) and downscaled at a 1-
251 km resolution using the delta method (Pastick et al., 2017). For the equilibrium run, the model was
252 driven using the averaged climate forcings from the 1901-1930 period for the study site location,
253 repeated continuously for a sufficient period so equilibrium of vegetation and below-ground C and N
254 fluxes and stocks was achieved. The resulting modeled ecosystem state for each site is then used to
255 initialize historical simulations. However, the calibration process described here only utilized outputs
256 from the equilibrium.

257 **2.5 MADS parameter calibration**

258 We employed the MADS software package for parameter calibration of DVM-DOS-TEM, aiming to
259 minimize the discrepancy between synthetic target and modeled data at the selected site (Barajas-Solano
260 et al., 2015; O'Malley and Vesselinov, 2015). Since its inception in 2010, MADS has undergone active
261 development, including a transition to the Julia programming language, which supports automatic
262 differentiation suitable for calibration problems(Vesselinov V.V., 2022).
263 The MADS package utilizes the Levenberg-Marquardt (LM) algorithm (Levenberg, 1944; Marquardt,
264 1963; Pujol, 2007) to minimize the difference (the sum of squared residuals) between observations and
265 modeled predictions. In SI1, we provide more details on the LM algorithm. The LM optimization
266 method designed to solve non-linear least squares optimization/minimization problems, which are
267 common in the field of history matching, model inversion, curve fitting, and parameter estimation. It
268 combines two approaches: the first-order steepest-descent gradient method and the second-order Gauss-
269 Newton method. This steepest-descent gradient method updates parameter values in the direction
270 opposite to the gradient, thereby it is generally efficient in finding local minima. The Gauss-Newton

271 method assumes that in a region close to the solution, the solved objective function behaves
272 quadratically.
273 The algorithm begins by selecting an initial estimate for the parameters that need to be optimized (Fig
274 S1). This initial guess is important as it sets the starting point for the optimization process. In our
275 experiment, the initial guess is randomly generated from within the provided range near `true`
276 parameter values. Alternatively, users can provide the initial guess. However, exploring a set of random
277 initial guesses provides an efficient approach to exploring the parameter space and discrimination
278 between local and global minima. In LM, we set the damping parameter (the Marquardt lambda) to
279 0.01. This parameter helps in adjusting the steps taken during the optimization process, balancing
280 between the two optimization strategies (the first- and the second order techniques discussed above).
281 The main advantages of the LM method are its robustness and minimal computational demand. It
282 effectively handles ill-conditioned problems where other optimization methods might fail (Lin et al.,
283 2016; Pujol, 2007). Additionally, for problems well-suited to the Gauss-Newton method, LM often
284 converges faster than gradient descent, making it an efficient choice for many non-linear least squares
285 problems.
286 The disadvantage of the LM method is its sensitivity to the initial parameter guesses, potentially
287 affecting its efficiency and convergence (Transtrum and Sethna, 2012). In these cases, MADS provides
288 alternative efficient approaches to address these computational challenges, such as (1) initializing the
289 calibration with random initial guesses, (2) multiple restarts of the LM algorithms throughout the
290 minimization process, and (3) exploration of a series of alternative values for various parameters
291 controlling LM performance (Lin et al., 2016). In addition, the compute speed deteriorates with the
292 higher number of parameters used in calibration. It requires the computation of the Jacobian matrix and
293 its pseudo-inverse, which can be computationally expensive for large-scale problems.
294

295 **2.6 Calibration Process, Parameters and Targets**

296 The calibration process in DVM-DOS-TEM is currently focused on the C and N annual cycles. Thus,
297 calibrated parameters are associated with and adjusted to the major C and N fluxes and stocks in the
298 vegetation and the soil. The calibration process follows a hierarchical approach (Figure 1), in which
299 parameters to be calibrated are organized in hierarchical levels associated with (1) model complexity
300 and feedback and (2) turnover of the processes the parameters are associated with. Therefore,
301 parameters related to vegetation dynamics are calibrated first, followed by the slowest soil-related
302 parameters.
303 The first step of the calibration relates to the simplest, fastest, first-order process in DVM-DOS-TEM,
304 and consists of adjusting the rate limiting parameter of maximum C assimilation of the vegetation
305 (c_{max}) driving vegetation GPP. Under baseline climate, the main limiting parameter of vegetation
306 productivity in the Arctic is N availability (Chapin and Kedrowski, 1983). Therefore, c_{max} is calibrated
307 to reproduce estimates of GPP from fertilization experiments where N limitation is ignored (GPP*).
308 When fertilization experiments are not available for the community/region of interest, GPP* is estimated
309 by applying a multiplicative factor to observed GPP under natural conditions. This multiplicative factor
310 is estimated from published fertilization experiments in similar communities and computed as the ratio

311 between GPP estimated in fertilized plots and GPP estimated in control plots. Based on the literature,
312 this fertilization factor can vary from 1.25 to 1.5 (Ruess et al., 1996; Shaver and Chapin, 1995).
313 The second step of the calibration process consists of turning on the representation of N limitation on
314 vegetation productivity in the model (Euskirchen et al., 2009) and calibrating the rest of the vegetation-
315 related parameters. In the current workflow, it consists of three substeps. These substeps could follow a
316 different order based on the preference of the user and the specifics of a given site. These are rate-
317 limiting parameters for maintenance respiration (Kr_b), maximum plant N uptake (n_{max}), C and N
318 litterfall (c_{fall} and n_{fall} respectively). These parameters are adjusted until DVM-DOS-TEM outputs
319 match observations of GPP and NPP, plant N uptake (Nup), and vegetation C and N pools,
320 respectively). Target values of these variables are listed in Table 1. It is important to note that the
321 parameters Kr_b, c_{fall}, and n_{fall}, as well as the variables for vegetation C and N, are specified per PFT
322 and per compartment (leaf, stem, root).
323 In the third step, the rate-limiting parameters of soil heterotrophic respiration (kdc) and rate of
324 microbial N uptake (n_{micb}^{up}) are calibrated as soil processes and takes longer to run in comparison to the
325 first two steps. These parameters are adjusted until DVM-DOS-TEM outputs match observations of soil
326 organic C and available N stocks. Target values of these variables are listed in Table 2. In a final state,
327 vegetation-related parameters are checked for a final adjustment after soil calibration, as soil processes
328 can feedback to vegetation dynamics.
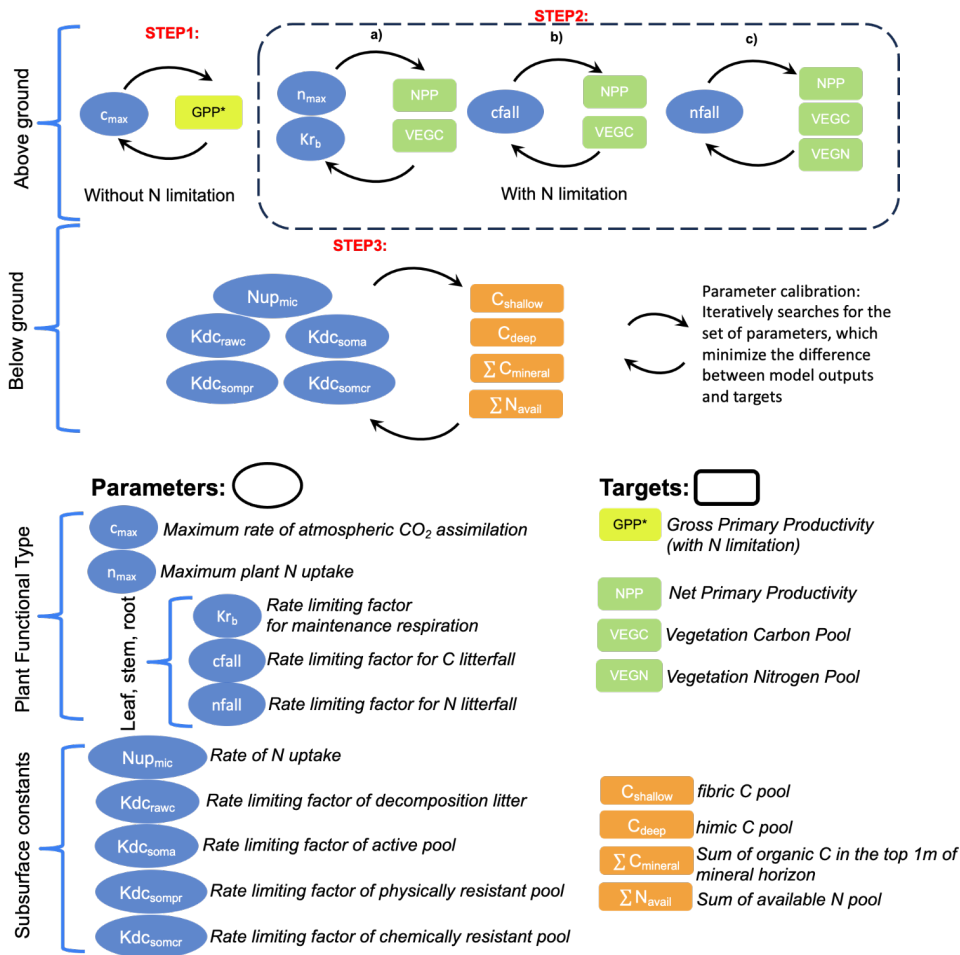
Figure 1. Schematics of the DVM-DOS-TEM model parameters and targets participated in the calibration process.

2.7 Calibrations setup and evaluation metric

Table 3 shows the parameter values used to calculate synthetic target values. We established four cases by perturbing the parameters by 10%, 20%, 50%, and 90% from their original values. For each case, the MADS calibration function randomly sampled ten sets of parameters within the specified ranges. These ten sets of randomly perturbed parameters were then optimized using the MADS algorithm. For each set of calibrated parameters and targets, we computed the root mean square error (RMSE) and relative error (RE) metrics. RMSE is employed to measure the magnitude of varying quantities, while RE gauges the absolute difference relative to the actual values. Given that some parameters are small (less than 10^{-3}), the relative error provides more informative insights. The following equations were used to compute these metrics:

$$RMSE = \sqrt{(\bar{x} - x)^2}\,, \tag{1}$$

$$RE = \left|\frac{\bar{x}-x}{x}\right| \cdot 100\%, \tag{2}$$

where $\bar{x}$ is the mean of the best five out of ten computed target/parameter matches and x is a synthetic target value.

To ensure the selection of the best-fitting parameters, we sorted error values from the lowest to the highest. Then, we selected the top five parameter sets, calculated their mean values, and compared these averaged parameters with the synthetic target values and known parameters.

Table 3: Synthetic parameter values for the black spruce forest site used in the parameter calibration process.

Name	Parameters	Units	Plant Functional Types			
			Evergreen Tree	Deciduous Shrub	Deciduous Tree	Moss
Maximum rate of atmospheric CO_2 assimilation	c_{max}	gC/m2/month	381.19	113.93	210.48	93.31
Maximum rate of plant N uptake	n_{max}	gN/m^2/month	3.38	1.55	1.0	3.55
rate limiting factor for C litterfall for leaf	c_{fall}^{leaf}	month^{-1}	0.0011	0.05	0.025	0.02
… for stem	c_{fall}^{stem}	month^{-1}	0.0034	0.0048	0.0036	
… for root	c_{fall}^{root}	month^{-1}	0.0052	0.0012	0.026	
Rate limiting factor for N litterfall for leaf	n_{fall}^{leaf}	month^{-1}	0.0102	0.045	0.018	0.007
… for stem	n_{fall}^{stem}	month^{-1}	0.001	0.001	0.005	
… for root	n_{fall}^{root}	month^{-1}	0.003	0.007	0.008	
Rate limiting factor for maintenance respiration for leaf	Kr_b^{leaf}	month^{-1}	-6.0	-3.45	-2.95	-4.65

… for stem	Kr_b^{stem}	month^{-1}	-4.88	-5.15	-6.65	
… for root	Kr_b^{root}	month^{-1}	-8.2	-6.2	-3.2	

349

350 **Table 4**: Synthetic below-ground target values for the black spruce forest site used in the parameter
351 calibration process

Name	Parameters	Unit	Value
Rate of microbial N uptake	n_{micb}^{up}	gg^{-1}	0.4495
Rate limiting factor of litter decomposition	kdc_{rawC}	$month^{-1}$	0.634
Rate limiting factor of active pool decomposition	kdc_{soma}	$month^{-1}$	0.54
Rate limiting factor of physically resistant pool decomposition	kdc_{sompr}	$month^{-1}$	0.002
Rate limiting factor of chemically resistant pool decomposition	kdc_{somcr}	$month^{-1}$	0.00007

352
353 **2.8 Application of the calibration method to observed target values**
354 After validating our calibration method with synthetic data, we applied it to observed at the Black
355 Spruce site. The observational dataset was compiled using a combination of in-situ measurements and
356 values from existing literature (Tables 5 and 6). Unlike synthetic targets, observed values inherently
357 carry uncertainty, which must be accounted for in the calibration process. The uncertainty range in the
358 observed targets varied from 27% to 40% (maximum coefficient of variation estimated from
359 observations reported in Melvin et al., 2015) influencing the final calibrated parameter estimates. After
360 calibrating parameters using observed means as targets, we sampled one thousand parameter sets
361 around the calibrated parameter set with a ±5% variation for all parameters excluding c_{max}. This
362 approach was implemented to increase the probability of achieving an optimal match with observations,
363 thereby allowing for a higher set of optimal parameter estimates. Additionally, this process enabled us
364 to evaluate the impact of calibrated soil parameters on vegetation-related target values, which were
365 calibrated over shorter time intervals.

366 **Table 5**: Observed vegetation target values at the black spruce forest site used in the parameter
367 calibration process. Standard deviations are indicated in parenthesis and estimated from field
368 measurements (n=15, Melvin et al., 2015).

Above-ground Target Names	Notation	Units	Plant Functional Types			
			Evergreen Tree	Deciduous Shrub	Deciduous Tree	Moss
Gross Primary Productivity without nitrogen limitation	GPP*	[gC/m²/year]	306.07 (±106)	24.53 (±8.4)	46.53 (±15.9)	54.23 (±18.5)
Net Primary Productivity	NPP	[gC/m²/year]	153.04 (±39)	12.27 (±3.9)	17.36 (±8.2)	27.10 (±11.1)
Vegetation Carbon Leaf	C_{leaf}	[gC/m²]	293.76 (±100)	15.13 (±5.4)	9.06 (±2.4)	180.85 (±93.3)
Vegetation Carbon Stem	C_{stem}	[gC/m²]	1796.32 (±706)	100.16 (±37)	333.75 (±185)	
Vegetation Carbon Root	C_{root}	[gC/m²]	404.48 (±177)	15.07 (±6.4)	44.8 (±15.9)	
Vegetation Nitrogen Leaf	N_{leaf}	[gC/m²]	6.35 (±3.5)	0.72 (±0.14)	0.7 (±0.2)	1.61 (±0.8)
Vegetation Nitrogen Stem	N_{stem}	[gC/m²]	24.34 (±11.3)	2.48 (±1)	9.45 (±4.9)	
Vegetation Nitrogen Root	N_{root}	[gC/m²]	0.17 (±0.04)	0.01	0.03 (±0.1)	

369

370 **Table 6**: Observed below-ground target values at the black spruce forest site used in the parameter
371 calibration process. Standard deviations are indicated in parenthesis and estimated from field
372 measurements (n=15, Melvin et al., 2015).

Below-ground Targets Names	Notation	Unit	Value
Carbon Shallow	$C_{shallow}$	g/m2	782.73 (±216.7)

Carbon Deep	C_{deep}	g/m2	3448.46 ($\pm$955)
Carbon Mineral Sum	$\sum C_{mineral}$	g/m2	41665.0 ($\pm$10580)
Available Nitrogen Sum	$\sum N_{avail}$	g/m2	0.76 ($\pm$0.24)

373

3 Results

3.1 Vegetation Targets

Depending on the range of parameter variance, our analysis revealed varying levels of accuracy between known synthetic parameters and those determined using the MADS search approach. In general, the variance between calibrated and synthetic values grew higher with a higher degree of parameter perturbation. The averaged RMSE values for all four PFTs showed similar increases (Figure 2) with an exception for $C_{stem}(c_{fall})$ deciduous shrubs, which made the RMSE score for the 10% variance higher than the 20% variance (Figure 2a and 2b). That is why we introduced the RE metric, which shows that the departure between synthetic and calibrated parameters increases with increasing perturbation and is the smallest for the 10% variance (Figure 3a). Additional analyses to explore the detailed relationship between parameter variance and RMSE for specific cases are presented in the supplementary materials (Figures S2-S5).

3.2 Vegetation Parameters

The RMSE for parameters was highest for Kr_b^{root} in the evergreen tree PFT (Figure 3). Overall, Kr_b and n_{max} parameters exhibited the worst recovery compared to other parameters based on the RMSE metric. Conversely, REs were highest for c_{fall} deciduous shrubs and less for Kr_b paramters. The RE indicated that smaller parameter values, such as n_{fall}, deviated more significantly from their synthetic values. Interestingly the RE score showed the same error range for 10% and 20% variance ranges, whereas RMSE showed that 10% variance has the smallest error.

3.3 Soil parameters

In general, the RMSE values for the sub-surface target parameters were relatively small but increased with a higher variance range (Figure 4). Notably, C_{deep} and $\sum C_{mineral}$ exhibited high RMSE values of 3.34 and 9.12, respectively, for the 10% variance range (Figure 4a). Despite this, the soil parameters for 10% variance showed the best match, with RMSE values less than 0.01. The RE for targets revealed increasing deviations from the synthetic parameter values for $\sum N_{avail}$. The RE for parameters indicated

399 that n_{micb}^{up}, kdc_{rawC} and kdc_{soma} had higher deviations from their respective synthetic values for the
400 50% and 90% variance range, respectively.

3.4 Comparison with Observations

402 Figure 5 shows a comparison between observed and modeled target values after calibration. Both
403 observed and modeled values were normalized by dividing by the highest value within their respective
404 groups (e.g., GPP, NPP). The highest difference (exceeding 20% uncertainty) was observed for
405 Evergreen Trees (Black Spruce). Notably, we encountered challenges in accurately matching the values
406 of the C_{stem} target and the values of N_{stem} (Figure 5a). Additionally, while the calibration method
407 struggled to align the carbon in the soil mineral pool, it captured other soil target values (Figure 5a).
408 Overall, the results demonstrate that the calibration approach is effective and reliable for optimizing
409 DVM-DOS-TEM model parameters.
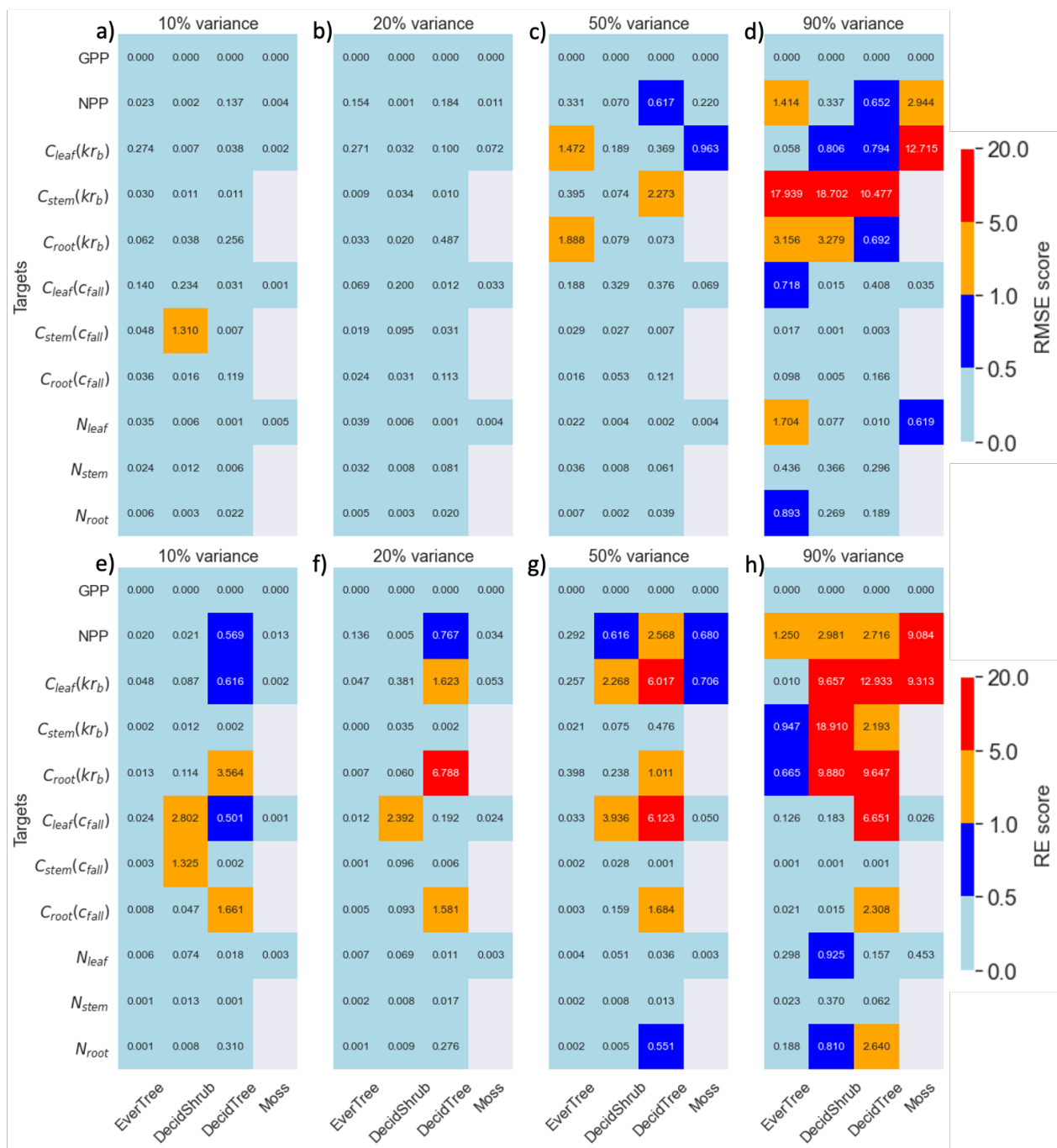
Figure 2. a), b), c), and d) are root mean square error (RMSE) metric and e), f), g), and h) are relative error (RE) metric for 10%, 20%, 50%, and 90% variance in the parameter range, correspondingly. Targets shown on y-axis, and plant functional types are on x-axis. The colorbar represents the RMSE and RE scores

410
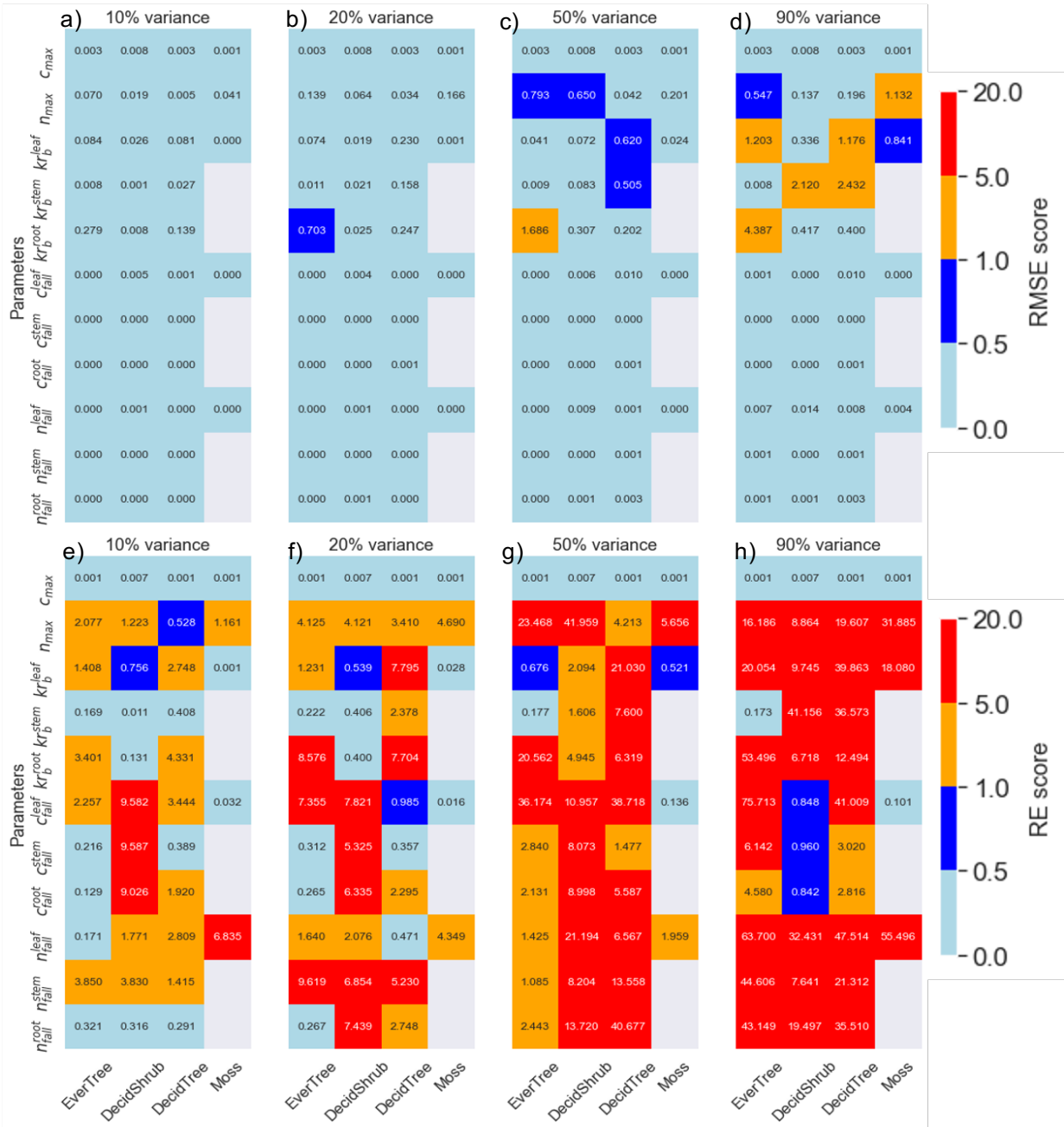
Figure 3. a), b), c), and d) are root mean square error (RMSE) metric and e), f), g), and h) are relative error (RE) metric for 10%, 20%, 50%, and 90% variance in the parameter range, correspondingly. DVM-DOS-TEM parameters shown on y-axis, and plant functional types are on x-axis. The colorbar represents the RMSE and RE scores.

411
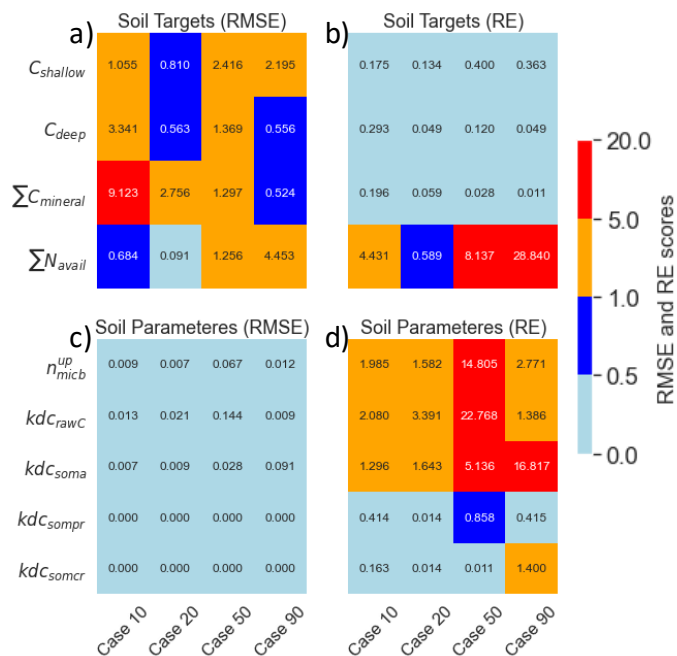
Figure 4. Comparison between calibrated and synthetic sub-surface target values (a) root mean square error (RMSE) and (b) relative error (RE) scores. Comparison between calibrated and synthetic sub-surface parameter values (a) root mean square error (RMSE) and (b) relative error (RE) scores for all range variances. The colorbar represents the RMSE and RE score.

412
413
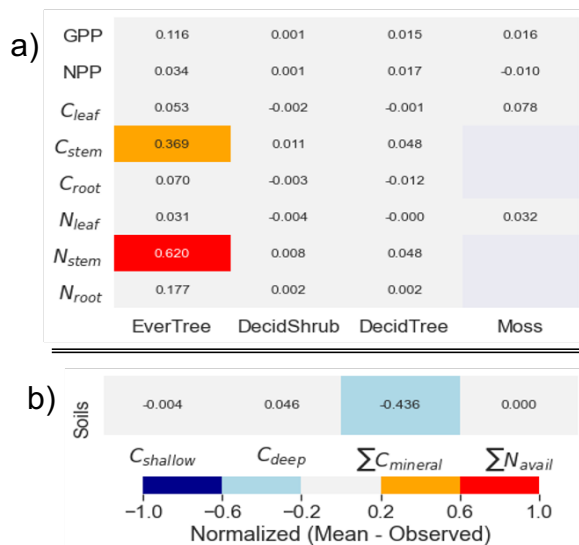
Figure 5. The comparison between observed and calibrated target values. The target values shown on y-axis, and plant functional types (a) and soil targets (b) on the x-axis. The colorbar represents the difference between normalized modeled and observed target values.

4 Discussion

Our findings highlight the challenges associated with calibrating carbon and nitrogen dynamics in high latitude permafrost ecosystems, particularly in accurately estimating carbon pools with slow turnover deep mineral soil carbon and allocation of partitioning carbon and nitrogen resources among within vegetation compartments to match in-situ observations closely. The strong interdependencies among parameters and state variables target values underscore the complexities of process-based modeling, reinforcing the need for automated calibration approaches like MADS to improve predictive accuracy.

4.1 Importance of the initial parameter guess

The initial parameter values, or initial guess, had minimal impact on the synthetic experiment, as the perturbed parameters were sufficiently close to the true values. However, for non-synthetic calibrations, the initial state is crucial, as starting with parameter values far from the true state can lead to non-convergence and significantly increase computation time(Nocedal and Wright, 2006). To address this, we developed parameter sensitivity methods to improve initial estimates (Briones et al., 2024). This approach utilized ensemble model simulations executed in parallel, systematically exploring parameter ranges through Latin hypercube sampling or uniform random sampling. By employing parallel processing before integrating parameters into the MADS calibration framework, we effectively refined initial estimates, minimized deviations from target values, and improved overall calibration efficiency.

4.2 Analysis of the recovery metrics

The mean parameter values calculated from the five best-matched MADS value predictions align closely with the synthetic parameter values, demonstrating the method's efficacy. The calculated REs for parameters indicate that the relative distance between the calibrated and the synthetic values increases with a higher parameter variance range, except RE for soil targets (Figure 4b, case 20%). For the soil targets, the RMSE for $\sum N_{avail}$ for 10% variance range were higher than 20% variance range. The higher RMSE for 10% variance than 20% variance range for vegetation-related targets as well as soil targets could be attributed to the limited number of cases (n=10) participated in each variance case. It is highly probable that increasing the total number of searches (higher than 10) would yield a more consistent pattern of decreasing accuracy with increasing variance.

4.3 Parameter-target relationship and small parameter values

The method demonstrated robust recovery of c_{max} values, indicating that it performs best when there is a linear relationship between parameters and target values (Eq. S1). For parameters, which do not exhibit a linear relationship with their target values (e.g. Kr_b, Eq. S4), the calibrated parameters showed wider variance. Additionally, small parameter values, such as n_{fall}, corresponded to small range of sampled values, leading to insensitivity between n_{fall} and vegetation N. To address this, we applied a logarithmic transformation to these and to some other small values for soil C rates.

4.4 The impact of n_{max} on N uptake and NPP

Sensitivity between model parameters and targets is crucial for effective parameter calibration. We observed that the sensitivity between n_{max} and NPP was not strong (Eq. S2, Eq. S5), which led us to

455 combine its calibration with the Kr_b parameter. Based on (Eq. S2), n_{max} directly influences N_{uptake}.
456 An increase in n_{max} enhances N_{uptake}, thereby increasing the total N supply. Since NPP is
457 proportional to N_{supply} and inversely proportional to $N_{required}$, a higher N supply can lead to a higher
458 NPP, provided that other factors remain constant. Therefore, despite the initial observation of weak
459 sensitivity, n_{max} could have a considerable impact on NPP due to its role in N_{uptake} and the overall
460 N_{supply}. However, our target values for plant N uptake are poorly constrained due to a lack of sufficient
461 observations. This underestimation of plant N uptake could account for the observed lack of sensitivity
462 of NPP to n_{max}. This issue requires further investigation and currently underscores the importance of
463 accurately calibrating n_{max} to ensure better simulation of ecosystem productivity.
464
465 **4.5 The Calibration Workflow**
466 Our findings indicate that calibrating one or two parameter sets at a time, while keeping other
467 parameters constant, is more effective than calibrating all parameters simultaneously. In the current
468 workflow, we combined n_{max} and Kr_b (Figure 1 Step a), which was based on the low sensitivity of
469 n_{max} to NPP. Combining multiple variables in one calibration step increases the compute time and
470 could result in low match accuracy. On the other hand, sequential parameter calibration carries the risk
471 of losing accuracy for parameters calibrated in previous steps. To mitigate this risk, we include targets
472 from previous calibration steps in the current calibration step. For example, when optimizing for n_{fall},
473 we include targets for NPP, vegetation C, and vegetation N.
474
475 Sequentially calibrating individual parameter sets is advantageous not only computationally but also in
476 preventing the occurrence of an underdetermined problem, which arise when the number of parameters
477 exceeds the number of targets. Undetermined problems exhibit a lower rate of convergence due to the
478 correlation between parameters and the sensitivity of multiple parameters to one or a few similar target
479 values. The study by Jafarov et al., (2020) showed that overdetermined problems with higher and
480 diverse number of target values, are more effective in recovering accurate parameter values.
481
482 **4.6 Sensitivity of the Kr_b parameter to NPP and vegetation C**
483 The Kr_b parameter exhibited higher sensitivity to both NPP and vegetation C compared to other
484 parameters. Despite the overall good model fitness, the deviation from the synthetic values for Kr_b was
485 higher. This was primarily due to Kr_b^{root} parameter for evergreen trees (Figure S3C) persistently
486 showed higher discrepancy. Its sensitivity can be explained by examining its role in the equations
487 governing maintenance respiration (R_m Eq. S3). The relationship between biomass and maintenance
488 respiration is non-linear; R_m increases as biomass increases, where Kr_b controls the intercept of this
489 relationship (Tian et al., 1999). Since NPP is computed as a resultant of GPP and autotrophic
490 respiration, including R_m, any alteration in Kr_b impacts NPP directly (Eq. S9). This sensitivity
491 underscores the importance of accurately calibrating Kr_b to ensure the correct simulation of ecosystem
492 productivity and C dynamics in the DVM-DOS-TEM.
493
494 **4.7 Vegetation and Below-Ground C stocks equilibrium time**

495   Due faster turnover, vegetation C and N stocks and fluxes equilibrate faster than soil C and N stocks
496   and fluxes. Thus we used a two-phase equilibration approach: 200 years for the vegetation and 2000
497   years for the soil. However, the C stocks achieved after 200 years of equilibration for vegetation might
498   shift when the model is run for an additional 1800 years to equilibrate soil. To mitigate this issue, we
499   developed equilibrium checks to ensure that the vegetation stocks remain stable and close to their
500   equilibrium values throughout the extended simulation period required for soil stocks equilibration.
501   These checks help identify significant departures from the initial equilibrium values of vegetation C and
502   N while allowing the model to run for a longer duration to achieve below-ground equilibrium. This
503   approach ensures the accuracy and stability of both vegetation and below-ground C and N stocks in
504   long-term model simulations.
505
506   **4.8 Observed target values**
507   The results of parameter calibration using site-specific observations indicate challenges in accurately
508   matching C_{stem} and N_{stem} target values for the evergreen plant functional type. This discrepancy could
509   be related to the allocation scheme of the model, attributing NPP resources to the various compartments
510   of the plant (Fox et al., 2018). Additionally, the model struggled to maintain the assigned carbon value
511   for $\sum C_{mineral}$. The difficulty in calibrating $C_{stem(E)}$ and $C_{root(E)}$ for evergreen trees can be partially
512   attributed to strong parameter interdependencies (see Figures SI7–SI10). For instance, $Kr_b^{leaf(E)}$
513   exhibits simultaneous correlations with both $C_{stem(E)}$ and $C_{root(E)}$ (Figure S7), while $c_{fall}^{stem(E)}$ shows an
514   inverse correlation with N leaf, stem, and root (Figure S8). These multi-target dependencies introduce
515   additional complexity, making it challenging to achieve a precise match for individual target values.
516   Similarly, the $\sum C_{mineral}$ target value is strongly influenced by kdc_{soma} and kdc_{sompr}, both of which
517   exert substantial control over C_{deep} and $\sum N_{avail}$ target values. These interactions underscore the
518   systemic constraints imposed by parameter interdependencies. Furthermore, this discrepancy could be
519   related to the functions controlling vertical transfers of carbon between horizons and the vertical
520   distribution of carbon quality (Harden et al., 2012). The model consistently showed that longer
521   equilibration times lead to a reduction in the mineral soil carbon pool. This was also observed by
522   Schaefer and Jafarov, (2016) in a different process-based ecosystem model, where they addressed the
523   issue by incorporating substrate availability constraints to prevent long-term carbon loss. Given the
524   complexity of these interdependencies, further investigation is needed, though it falls beyond the scope
525   of this study.
526   The calibration of rate-limiting soil parameters that influence C and N stocks and turnover directly
527   impacts vegetation productivity by modulating nitrogen availability. Figure S10 shows a significant
528   correlation between microbial nitrogen uptake and $C_{leaf(DS)}$ of deciduous shrub, highlighting the
529   interaction between soil processes and vegetation-related parameters. While long-term soil parameter
530   calibration inherently feedbacks into vegetation dynamics, the most substantial changes in vegetation-
531   related parameters typically occur during short-term model runs, resulting in minimal net changes over
532   extended simulations.
533
534   **4.9 Limitations**

There are cases where the model fails to accurately match target values due to poor data quality or its inability to fully represent certain ecological processes (Dietze et al., 2018; Luo et al., 2016). Large discrepancies between observed and modeled targets can hinder the convergence of the LM method, requiring more iterations and leading to suboptimal agreement with observations. As previously mentioned, starting with well-constrained initial parameter estimates can mitigate this issue, which can be achieved by performing sensitivity analyses to identify the most influential parameters and refine their ranges prior to calibration (Efstratiadis and Koutsoyiannis, 2010).

Additionally, calibrating soil-related parameters is computationally demanding, often resulting in a substantial slowdown of the overall calibration workflow. Machine learning (ML) models offer a promising solution by acting as surrogate models to approximate the equilibrium state, thereby reducing the computational burden (Fer et al., 2018; Reichstein et al., 2019). However, implementing such approaches necessitates large training datasets, often requiring thousands of model simulations to achieve reliable predictions. Future research should explore the integration of ML-based calibration techniques into the workflow, which could significantly enhance computational efficiency and further improve model accuracy (Castelletti et al., 2012; Dagon et al., 2020).

5. Conclusion

In this study, we showed that the developed MADS parameter calibration method for the DVM-DOS-TEM can effectively recover the synthetic parameter set, optimizing labor and time, and enhancing reproducibility of the calibration process. By implementing a structured workflow that calibrates one or two parameters at a time and including equilibrium checks the method ensured accurate parameter estimation even for high variance parameter range. The primary advantage of the semi-automated MADS calibration approach is its significant enhancement of repeatability and clear quantification of calibration performance. In contrast, manual calibration processes are often difficult to reproduce as it is impractical if not impossible, to record users continuous adjustments to parameters values until improved results are achieved. Additionally, appreciation of model improvement by the user is often subjective as running a statistical evaluation at each parameter adjustment would be too time consuming. In the approach demonstrated in this study, we introduced a calibration metric that provides a quantifiable measure of the overall quality of the calibration. This metric enhances reproducibility by allowing future users working on the same site to follow the established workflow and reliably reproduce the calibrated parameter and target values. The RMSE quantifies the average differences between calibrated and observed (synthetic) values, while the RE metric indicates deviations from the synthetic values.

In all calibration experiments, we utilized only ten randomly perturbed initial parameter sets within a specified variance range. Our results indicated that perturbation ranges of 10%-20% were equally effective in achieving optimal target/parameter calibration. However, increasing the number of random perturbations could potentially shift the statistics, favoring a 10% variance range.

While the choice of the initial guess is crucial, its impact was mitigated in our study due to the design involving variance around synthetic parameter values. The developed method significantly reduces the labor and time required for calibrating DVM-DOS-TEM model parameters. However, it does not entirely replace the need for human intervention. Users still need to understand the specifics of the model and the relationship between parameters and targets, as well as conduct post-processing assessments of the fit. In future work, we will apply this method to data processed at multiple study sites to validate further and refine the calibration approach.

The application of the calibration method to site-specific observations revealed challenges in accurately matching C_{stem}, N_{stem} and $\sum C_{mineral}$ values, primarily due to parameter interdependencies and data uncertainties. Discrepancies between observed and modeled target values exceeded the known the measurement uncertainty, suggesting that structural uncertainty within the model may contribute to these deviations. This indicates a potential need for a more detailed representation of ecological processes to improve model accuracy. However, these challenges may be site-specific and may not necessarily apply to other ecosystem types. Despite these limitations, the study demonstrates the effectiveness and reliability of the calibration approach while identifying key areas for future model refinement.

6. Data and model availability

The version of the model used in these simulations, along with the calibration scripts, auxiliary files (including plots presented in the paper), and corresponding output files, is available in Jafarov, (2024).

7. Author contributions

EEJ designed and executed the experiment. HG supervised in experiment design. VV supervised with MADS model. RR, TC, and DT provided technical support on the DVM-DOS-TEM model. VB, AK, ALM, BM, C-CC, and JC tested calibration approach. TS technical support on scientific computing. All authors participated in manuscript writing and editing. SMN and BMR provided overall supervision and research funding.

8. Competing interests

The contact author has declared that none of the authors has any competing interests.

9. Disclaimer

Publisher's note: Copernicus Publications remains neutral with regard to jurisdictional claims in published maps and institutional affiliations.

10. Acknowledgments

This work was supported by the Quadrature Climate Foundation (grant number 01-21-000094) and catalyzed through the Audacious Project (Permafrost Pathways) to SMN and BMR.

11. References

Andresen, C. G., Lawrence, D. M., Wilson, C. J., McGuire, A. D., Koven, C., Schaefer, K., Jafarov, E., Peng, S., Chen, X., Gouttevin, I., Burke, E., Chadburn, S., Ji, D., Chen, G., Hayes, D., and Zhang, W.: Soil moisture and hydrology projections of the permafrost region – a model intercomparison, The Cryosphere, 14, 445–459, https://doi.org/10.5194/tc-14-445-2020, 2020.

Barajas-Solano, D. A., Wohlberg, B. E., Vesselinov, V. V., and Tartakovsky, D. M.: Linear functional minimization for inverse modeling, Water Resources Research, 51, 4516–4531, https://doi.org/10.1002/2014WR016179, 2015.

Beven, K. and Freer, J.: Equifinality, data assimilation, and uncertainty estimation in mechanistic modelling of complex environmental systems using the GLUE methodology, Journal of Hydrology, 249, 11–29, https://doi.org/10.1016/S0022-1694(01)00421-8, 2001.

Birch, L., Schwalm, C. R., Natali, S., Lombardozzi, D., Keppel-Aleks, G., Watts, J., Lin, X., Zona, D., Oechel, W., Sachs, T., Black, T. A., and Rogers, B. M.: Addressing biases in Arctic–boreal carbon cycling in the Community Land Model Version 5, Geosci. Model Dev., 14, 3361–3382, https://doi.org/10.5194/gmd-14-3361-2021, 2021.

Bloom, A. A., Exbrayat, J.-F., Van Der Velde, I. R., Feng, L., and Williams, M.: The decadal state of the terrestrial carbon cycle: Global retrievals of terrestrial carbon allocation, pools, and residence times, Proc. Natl. Acad. Sci. U.S.A., 113, 1285–1290, https://doi.org/10.1073/pnas.1515160113, 2016.

Briones, V., Jafarov, E. E., Genet, H., Rogers, B. M., Rutter, R. M., Carman, T. B., Clein, J., Euschkirchen, E. S., Schuur, E. A., Watts, J. D., and Natali, S. M.: Exploring the interplay between soil thermal and hydrological changes and their impact on carbon fluxes in permafrost ecosystems, Environ. Res. Lett., 19, 074003, https://doi.org/10.1088/1748-9326/ad50ed, 2024.

Brunetti, G., Šimunek, J., Wöhling, T., and Stumpp, C.: An in-depth analysis of Markov-Chain Monte Carlo ensemble samplers for inverse vadose zone modeling, Journal of Hydrology, 624, 129822, https://doi.org/10.1016/j.jhydrol.2023.129822, 2023.

Calef, M. P., David McGuire, A., Epstein, H. E., Scott Rupp, T., and Shugart, H. H.: Analysis of vegetation distribution in Interior Alaska and sensitivity to climate change using a logistic regression approach, Journal of Biogeography, 32, 863–878, https://doi.org/10.1111/j.1365-2699.2004.01185.x, 2005.

Castelletti, A., Galelli, S., Ratto, M., Soncini-Sessa, R., and Young, P. C.: A general framework for Dynamic Emulation Modelling in environmental problems, Environmental Modelling & Software, 34, 5–18, https://doi.org/10.1016/j.envsoft.2012.01.002, 2012.

Chapin, F. S. and Kedrowski, R. A.: Seasonal Changes in Nitrogen and Phosphorus Fractions and Autumn Retranslocation in Evergreen and Deciduous Taiga Trees, Ecology, 64, 376–391, https://doi.org/10.2307/1937083, 1983.

Dagon, K., Sanderson, B. M., Fisher, R. A., and Lawrence, D. M.: A machine learning approach to emulation and biophysical parameter estimation with the Community Land Model, version 5, Adv. Stat. Clim. Meteorol. Oceanogr., 6, 223–244, https://doi.org/10.5194/ascmo-6-223-2020, 2020.

Dietze, M. C., Fox, A., Beck-Johnson, L. M., Betancourt, J. L., Hooten, M. B., Jarnevich, C. S., Keitt, T. H., Kenney, M. A., Laney, C. M., Larsen, L. G., Loescher, H. W., Lunch, C. K., Pijanowski, B. C., Randerson, J. T., Read, E. K., Tredennick, A. T., Vargas, R., Weathers, K. C., and White, E. P.: Iterative near-term ecological forecasting: Needs, opportunities, and challenges, Proc. Natl. Acad. Sci. U.S.A., 115, 1424–1432, https://doi.org/10.1073/pnas.1710231115, 2018.

Efstratiadis, A. and Koutsoyiannis, D.: One decade of multi-objective calibration approaches in hydrological modelling: a review, Hydrological Sciences Journal, 55, 58–78, https://doi.org/10.1080/02626660903526292, 2010.

Euskirchen, E. S., McGUIRE, A. D., Kicklighter, D. W., Zhuang, Q., Clein, J. S., Dargaville, R. J., Dye, D. G., Kimball, J. S., McDONALD, K. C., Melillo, J. M., Romanovsky, V. E., and Smith, N. V.: Importance of recent shifts in soil thermal dynamics on growing season length, productivity, and carbon sequestration in terrestrial high-latitude ecosystems: HIGH-LATITUDE CLIMATE CHANGE INDICATORS, Global Change Biology, 12, 731–750, https://doi.org/10.1111/j.1365-2486.2006.01113.x, 2006.

Euskirchen, E. S., McGuire, A. D., Chapin, F. S., Yi, S., and Thompson, C. C.: Changes in vegetation in northern Alaska under scenarios of climate change, 2003–2100: implications for climate feedbacks, Ecological Applications, 19, 1022–1043, https://doi.org/10.1890/08-0806.1, 2009.

Euskirchen, E. S., Edgar, C. W., Turetsky, M. R., Waldrop, M. P., and Harden, J. W.: Differential response of carbon fluxes to climate in three peatland ecosystems that vary in the presence and stability of permafrost: Carbon fluxes and permafrost thaw, J. Geophys. Res. Biogeosci., 119, 1576–1595, https://doi.org/10.1002/2014JG002683, 2014.

Euskirchen, E. S., Serbin, S. P., Carman, T. B., Fraterrigo, J. M., Genet, H., Iversen, C. M., Salmon, V., and McGuire, A. D.: Assessing dynamic vegetation model parameter uncertainty across Alaskan arctic tundra plant communities, Ecological Applications, 32, https://doi.org/10.1002/eap.2499, 2022.

Fer, I., Kelly, R., Moorcroft, P. R., Richardson, A. D., Cowdery, E. M., and Dietze, M. C.: Linking big models to big data: efficient ecosystem model calibration through Bayesian model emulation, Biogeosciences, 15, 5801–5830, https://doi.org/10.5194/bg-15-5801-2018, 2018.

Fisher, R. A. and Koven, C. D.: Perspectives on the Future of Land Surface Models and the Challenges of Representing Complex Terrestrial Systems, J Adv Model Earth Syst, 12, e2018MS001453, https://doi.org/10.1029/2018MS001453, 2020.

Forrester, A. I. J., Bressloff, N. W., and Keane, A. J.: Optimization using surrogate models and partially converged computational fluid dynamics simulations, Proc. R. Soc. A., 462, 2177–2204, https://doi.org/10.1098/rspa.2006.1679, 2006.

Fox, A. M., Hoar, T. J., Anderson, J. L., Arellano, A. F., Smith, W. K., Litvak, M. E., MacBean, N., Schimel, D. S., and Moore, D. J. P.: Evaluation of a Data Assimilation System for Land Surface Models Using CLM4.5, J Adv Model Earth Syst, 10, 2471–2494, https://doi.org/10.1029/2018MS001362, 2018.

Genet, H., McGuire, A. D., Barrett, K., Breen, A., Euskirchen, E. S., Johnstone, J. F., Kasischke, E. S., Melvin, A. M., Bennett, A., Mack, M. C., Rupp, T. S., Schuur, A. E. G., Turetsky, M. R., and Yuan, F.: Modeling the effects of fire severity and climate warming on active layer thickness and soil carbon storage of black spruce forests across the landscape in interior Alaska, Environ. Res. Lett., 8, 045016, https://doi.org/10.1088/1748-9326/8/4/045016, 2013.

Genet, H., He, Y., Lyu, Z., McGuire, A. D., Zhuang, Q., Clein, J., D'Amore, D., Bennett, A., Breen, A., Biles, F., Euskirchen, E. S., Johnson, K., Kurkowski, T., (Kushch) Schroder, S., Pastick, N., Rupp, T. S., Wylie, B., Zhang, Y., Zhou, X., and Zhu, Z.: The role of driving factors in historical and projected carbon dynamics of upland ecosystems in Alaska, Ecol Appl, 28, 5–27, https://doi.org/10.1002/eap.1641, 2018.

Hansen, P. C.: Rank-Deficient and Discrete Ill-Posed Problems: Numerical Aspects of Linear Inversion, Society for Industrial and Applied Mathematics, https://doi.org/10.1137/1.9780898719697, 1998.

Harden, J. W., Koven, C. D., Ping, C., Hugelius, G., David McGuire, A., Camill, P., Jorgenson, T., Kuhry, P., Michaelson, G. J., O'Donnell, J. A., Schuur, E. A. G., Tarnocai, C., Johnson, K., and Grosse, G.: Field information links permafrost carbon to physical vulnerabilities of thawing, Geophysical Research Letters, 39, 2012GL051958, https://doi.org/10.1029/2012GL051958, 2012.

Harp, D. R., Atchley, A. L., Painter, S. L., Coon, E. T., Wilson, C. J., Romanovsky, V. E., and Rowland, J. C.: Effect of soil property uncertainties on permafrost thaw projections: a calibration-constrained analysis, The Cryosphere, 10, 341–358, https://doi.org/10.5194/tc-10-341-2016, 2016.

Harris, I., Jones, P. D., Osborn, T. J., and Lister, D. H.: Updated high-resolution grids of monthly climatic observations - the CRU TS3.10 Dataset: UPDATED HIGH-RESOLUTION GRIDS OF MONTHLY CLIMATIC OBSERVATIONS, Int. J. Climatol., 34, 623–642, https://doi.org/10.1002/joc.3711, 2014.

Hugelius, G., Strauss, J., Zubrzycki, S., Harden, J. W., Schuur, E. A. G., Ping, C.-L., Schirrmeister, L., Grosse, G., Michaelson, G. J., Koven, C. D., O'Donnell, J. A., Elberling, B., Mishra, U., Camill, P., Yu, Z., Palmtag, J., and Kuhry, P.: Estimated stocks of circumpolar permafrost carbon with quantified uncertainty ranges and identified data gaps, Biogeosciences, 11, 6573–6593, https://doi.org/10.5194/bg-11-6573-2014, 2014.

Jafarov, E.: Estimation of above- and below-ground ecosystem parameters for the DVM-DOS-TEM v0.7.0 model using MADS v1.7.3: a synthetic case study, , https://doi.org/10.5281/ZENODO.13772987, 2024.

Jafarov, E. E., Romanovsky, V. E., Genet, H., McGuire, A. D., and Marchenko, S. S.: The effects of fire on the thermal stability of permafrost in lowland and upland black spruce forests of interior Alaska in a changing climate, Environ. Res. Lett., 8, 035030, https://doi.org/10.1088/1748-9326/8/3/035030, 2013.

Jafarov, E. E., Nicolsky, D. J., Romanovsky, V. E., Walsh, J. E., Panda, S. K., and Serreze, M. C.: The effect of snow: How to better model ground surface temperatures, Cold Regions Science and Technology, 102, 63–77, https://doi.org/10.1016/j.coldregions.2014.02.007, 2014.

Jafarov, E. E., Harp, D. R., Coon, E. T., Dafflon, B., Tran, A. P., Atchley, A. L., Lin, Y., and Wilson, C. J.: Estimation of subsurface porosities and thermal conductivities of polygonal tundra by coupled inversion of electrical resistivity, temperature, and moisture content data, The Cryosphere, 14, 77–91, https://doi.org/10.5194/tc-14-77-2020, 2020.

Jean, M., Melvin, A. M., Mack, M. C., and Johnstone, J. F.: Broadleaf Litter Controls Feather Moss Growth in Black Spruce and Birch Forests of Interior Alaska, Ecosystems, 23, 18–33, https://doi.org/10.1007/s10021-019-00384-8, 2020.

Kelly, R., Chipman, M. L., Higuera, P. E., Stefanova, I., Brubaker, L. B., and Hu, F. S.: Recent burning of boreal forests exceeds fire regime limits of the past 10,000 years, Proc. Natl. Acad. Sci. U.S.A., 110, 13055–13060, https://doi.org/10.1073/pnas.1305069110, 2013.

Koven, C. D., Lawrence, D. M., and Riley, W. J.: Permafrost carbon–climate feedback is sensitive to deep soil carbon decomposability but not deep soil nitrogen dynamics, Proc. Natl. Acad. Sci. U.S.A., 112, 3752–3757, https://doi.org/10.1073/pnas.1415123112, 2015.

Koziel, S., Ciaurri, D. E., and Leifsson, L.: Surrogate-Based Methods, in: Computational Optimization, Methods and Algorithms, vol. 356, edited by: Koziel, S. and Yang, X.-S., Springer Berlin Heidelberg, Berlin, Heidelberg, 33–59, https://doi.org/10.1007/978-3-642-20859-1_3, 2011.

Lara, M. J., Genet, H., McGuire, A. D., Euskirchen, E. S., Zhang, Y., Brown, D. R. N., Jorgenson, M. T., Romanovsky, V., Breen, A., and Bolton, W. R.: Thermokarst rates intensify due to climate change and forest fragmentation in an Alaskan boreal forest lowland, Global Change Biology, 22, 816–829, https://doi.org/10.1111/gcb.13124, 2016.

Lawrence, D. M., Koven, C. D., Swenson, S. C., Riley, W. J., and Slater, A. G.: Permafrost thaw and resulting soil moisture changes regulate projected high-latitude CO_2 and CH_4 emissions, Environ. Res. Lett., 10, 094011, https://doi.org/10.1088/1748-9326/10/9/094011, 2015.

Levenberg, K.: A METHOD FOR THE SOLUTION OF CERTAIN NON-LINEAR PROBLEMS IN LEAST SQUARES, Quarterly of Applied Mathematics, 2, 164–168, 1944.

Lin, Y., O'Malley, D., and Vesselinov, V. V.: A computationally efficient parallel L evenberg- M arquardt algorithm for highly parameterized inverse model analyses, Water Resources Research, 52, 6948–6977, https://doi.org/10.1002/2016WR019028, 2016.

Linde, N., Renard, P., Mukerji, T., and Caers, J.: Geological realism in hydrogeological and geophysical inverse modeling: A review, Advances in Water Resources, 86, 86–101, https://doi.org/10.1016/j.advwatres.2015.09.019, 2015.

Ling, X.-L., Fu, C.-B., Yang, Z.-L., and Guo, W.-D.: Comparison of different sequential assimilation algorithms for satellite-derived leaf area index using the Data Assimilation Research Testbed (version Lanai), Geosci. Model Dev., 12, 3119–3133, https://doi.org/10.5194/gmd-12-3119-2019, 2019.

Luo, Y., Ahlström, A., Allison, S. D., Batjes, N. H., Brovkin, V., Carvalhais, N., Chappell, A., Ciais, P., Davidson, E. A., Finzi, A., Georgiou, K., Guenet, B., Hararuk, O., Harden, J. W., He, Y., Hopkins, F., Jiang, L., Koven, C., Jackson, R. B., Jones, C. D., Lara, M. J., Liang, J., McGuire, A. D., Parton, W., Peng, C., Randerson, J. T., Salazar, A., Sierra, C. A., Smith, M. J., Tian, H., Todd-Brown, K. E. O., Torn, M., Van Groenigen, K. J., Wang, Y. P., West, T. O., Wei, Y., Wieder, W. R., Xia, J., Xu, X., Xu, X., and Zhou, T.: Toward more realistic projections of soil carbon dynamics by Earth system models, Global Biogeochemical Cycles, 30, 40–56, https://doi.org/10.1002/2015GB005239, 2016.

MacBean, N., Peylin, P., Chevallier, F., Scholze, M., and Schürmann, G.: Consistent assimilation of multiple data streams in a carbon cycle dataassimilation system, Geosci. Model Dev., 9, 3569–3588, https://doi.org/10.5194/gmd-9-3569-2016, 2016.

Marquardt, D. W.: An Algorithm for Least-Squares Estimation of Nonlinear Parameters, Journal of the Society for Industrial and Applied Mathematics, 11, 431–441, 1963.

Matthes, et al: Advances in Permafrost Representation: Biophysical Processes in Earth System Models and the Role of Offline Models., Permafrost and Periglac Process., https://doi.org/10.1002/ppp.2269, 2025.

McGuire, A. D., Koven, C., Lawrence, D. M., Clein, J. S., Xia, J., Beer, C., Burke, E., Chen, G., Chen, X., Delire, C., Jafarov, E., MacDougall, A. H., Marchenko, S., Nicolsky, D., Peng, S., Rinke, A., Saito, K., Zhang, W., Alkama, R., Bohn, T. J., Ciais, P., Decharme, B., Ekici, A., Gouttevin, I., Hajima, T., Hayes, D. J., Ji, D., Krinner, G., Lettenmaier, D. P., Luo, Y., Miller, P. A., Moore, J. C., Romanovsky, V., Schädel, C., Schaefer, K., Schuur, E. A. G., Smith, B., Sueyoshi, T., and Zhuang, Q.: Variability in the sensitivity among model simulations of permafrost and carbon dynamics in the permafrost region between 1960 and 2009: MODELING PERMAFROST CARBON DYNAMICS, Global Biogeochem. Cycles, 30, 1015–1037, https://doi.org/10.1002/2016GB005405, 2016.

McGuire, A. D., Lawrence, D. M., Koven, C., Clein, J. S., Burke, E., Chen, G., Jafarov, E., MacDougall, A. H., Marchenko, S., Nicolsky, D., Peng, S., Rinke, A., Ciais, P., Gouttevin, I., Hayes, D. J., Ji, D., Krinner, G., Moore, J. C., Romanovsky, V., Schädel, C., Schaefer, K., Schuur, E. A. G., and Zhuang, Q.: Dependence of the evolution of carbon dynamics in the northern permafrost region on the trajectory of climate change, Proc Natl Acad Sci USA, 115, 3882–3887, https://doi.org/10.1073/pnas.1719903115, 2018.

Melvin, A. M., Mack, M. C., Johnstone, J. F., David McGuire, A., Genet, H., and Schuur, E. A. G.: Differences in Ecosystem Carbon Distribution and Nutrient Cycling Linked to Forest Tree Species Composition in a Mid-Successional Boreal Forest, Ecosystems, 18, 1472–1488, https://doi.org/10.1007/s10021-015-9912-7, 2015.

Mishra, U., Hugelius, G., Shelef, E., Yang, Y., Strauss, J., Lupachev, A., Harden, J. W., Jastrow, J. D., Ping, C.-L., Riley, W. J., Schuur, E. A. G., Matamala, R., Siewert, M., Nave, L. E., Koven, C. D., Fuchs, M., Palmtag, J., Kuhry, P., Treat, C. C.,

Zubrzycki, S., Hoffman, F. M., Elberling, B., Camill, P., Veremeeva, A., and Orr, A.: Spatial heterogeneity and environmental predictors of permafrost region soil organic carbon stocks, Sci. Adv., 7, eaaz5236, https://doi.org/10.1126/sciadv.aaz5236, 2021.

Natali, S. M., Holdren, J. P., Rogers, B. M., Treharne, R., Duffy, P. B., Pomerance, R., and MacDonald, E.: Permafrost carbon feedbacks threaten global climate goals, Proc. Natl. Acad. Sci. U.S.A., 118, e2100163118, https://doi.org/10.1073/pnas.2100163118, 2021.

Nicolsky, D. J., Romanovsky, V. E., and Tipenko, G. S.: Using in-situ temperature measurements to estimate saturated soil thermal properties by solving a sequence of optimization problems, The Cryosphere, 1, 41–58, https://doi.org/10.5194/tc-1-41-2007, 2007.

Nicolsky, D. J., Romanovsky, V. E., and Panteleev, G. G.: Estimation of soil thermal properties using in-situ temperature measurements in the active layer and permafrost, Cold Regions Science and Technology, 55, 120–129, https://doi.org/10.1016/j.coldregions.2008.03.003, 2009.

Nocedal, J. and Wright, S.: Numerical Optimization, Springer New York, https://doi.org/10.1007/978-0-387-40065-5, 2006.

O'Malley, D. and Vesselinov, V. V.: Bayesian-information-gap decision theory with an application to CO_2 sequestration: BAYESIAN-INFORMATION-GAP DECISION THEORY, Water Resour. Res., 51, 7080–7089, https://doi.org/10.1002/2015WR017413, 2015.

Pastick, N. J., Duffy, P., Genet, H., Rupp, T. S., Wylie, B. K., Johnson, K. D., Jorgenson, M. T., Bliss, N., McGuire, A. D., Jafarov, E. E., and Knight, J. F.: Historical and projected trends in landscape drivers affecting carbon dynamics in Alaska, Ecological Applications, 27, 1383–1402, https://doi.org/10.1002/eap.1538, 2017.

Peylin, P., Bacour, C., MacBean, N., Leonard, S., Rayner, P., Kuppel, S., Koffi, E., Kane, A., Maignan, F., Chevallier, F., Ciais, P., and Prunet, P.: A new stepwise carbon cycle data assimilation system using multiple data streams to constrain the simulated land surface carbon cycle, Geosci. Model Dev., 9, 3321–3346, https://doi.org/10.5194/gmd-9-3321-2016, 2016.

Pujol, J.: The solution of nonlinear inverse problems and the Levenberg-Marquardt method, GEOPHYSICS, 72, W1–W16, https://doi.org/10.1190/1.2732552, 2007.

Queipo, N. V., Haftka, R. T., Shyy, W., Goel, T., Vaidyanathan, R., and Kevin Tucker, P.: Surrogate-based analysis and optimization, Progress in Aerospace Sciences, 41, 1–28, https://doi.org/10.1016/j.paerosci.2005.02.001, 2005.

Razavi, S., Tolson, B. A., and Burn, D. H.: Review of surrogate modeling in water resources, Water Resources Research, 48, 2011WR011527, https://doi.org/10.1029/2011WR011527, 2012.

Regis, R. G. and Shoemaker, C. A.: A Stochastic Radial Basis Function Method for the Global Optimization of Expensive Functions, INFORMS Journal on Computing, 19, 497–509, https://doi.org/10.1287/ijoc.1060.0182, 2007.

Reichstein, M., Camps-Valls, G., Stevens, B., Jung, M., Denzler, J., Carvalhais, N., and Prabhat: Deep learning and process understanding for data-driven Earth system science, Nature, 566, 195–204, https://doi.org/10.1038/s41586-019-0912-1, 2019.

Ruess, R. W., Cleve, K. V., Yarie, J., and Viereck, L. A.: Contributions of fine root production and turnover to the carbon and nitrogen cycling in taiga forests of the Alaskan interior, Can. J. For. Res., 26, 1326–1336, https://doi.org/10.1139/x26-148, 1996.

Rykiel, E. J.: Testing ecological models: the meaning of validation, Ecological Modelling, 90, 229–244, https://doi.org/10.1016/0304-3800(95)00152-2, 1996.

Schädel, C., Rogers, B. M., Lawrence, D. M., Koven, C. D., Brovkin, V., Burke, E. J., Genet, H., Huntzinger, D. N., Jafarov, E., McGuire, A. D., Riley, W. J., and Natali, S. M.: Earth system models must include permafrost carbon processes, Nat. Clim. Chang., https://doi.org/10.1038/s41558-023-01909-9, 2024.

Schaefer, K. and Jafarov, E.: A parameterization of respiration in frozen soils based on substrate availability, Biogeosciences, 13, 1991–2001, https://doi.org/10.5194/bg-13-1991-2016, 2016.

Scholze, M., Kaminski, T., Knorr, W., Blessing, S., Vossbeck, M., Grant, J. P., and Scipal, K.: Simultaneous assimilation of SMOS soil moisture and atmospheric CO2 in-situ observations to constrain the global terrestrial carbon cycle, Remote Sensing of Environment, 180, 334–345, https://doi.org/10.1016/j.rse.2016.02.058, 2016.

Schürmann, G. J., Kaminski, T., Köstler, C., Carvalhais, N., Voßbeck, M., Kattge, J., Giering, R., Rödenbeck, C., Heimann, M., and Zaehle, S.: Constraining a land-surface model with multiple observations by application of the MPI-Carbon Cycle Data Assimilation System V1.0, Geosci. Model Dev., 9, 2999–3026, https://doi.org/10.5194/gmd-9-2999-2016, 2016.

Schuur, E. A. G., Abbott, B. W., Commane, R., Ernakovich, J., Euskirchen, E., Hugelius, G., Grosse, G., Jones, M., Koven, C., Leshyk, V., Lawrence, D., Loranty, M. M., Mauritz, M., Olefeldt, D., Natali, S., Rodenhizer, H., Salmon, V., Schädel, C., Strauss, J., Treat, C., and Turetsky, M.: Permafrost and Climate Change: Carbon Cycle Feedbacks From the Warming Arctic, Annu. Rev. Environ. Resour., 47, 343–371, https://doi.org/10.1146/annurev-environ-012220-011847, 2022.

Shaver, G. R. and Chapin, F. S.: Long-term responses to factorial, NPK fertilizer treatment by Alaskan wet and moist tundra sedge species, Ecography, 18, 259–275, https://doi.org/10.1111/j.1600-0587.1995.tb00129.x, 1995.

Tian, H., Melillo, J. M., Kicklighter, D. W., McGuire, A. D., and Helfrich, J.: The sensitivity of terrestrial carbon storage to historical climate variability and atmospheric CO_2 in the United States, Tellus B: Chemical and Physical Meteorology, 51, 414, https://doi.org/10.3402/tellusb.v51i2.16318, 1999.

Tran, A. P., Dafflon, B., and Hubbard, S. S.: Coupled land surface–subsurface hydrogeophysical inverse modeling to estimate soil organic carbon content and explore associated hydrological and thermal dynamics in the Arctic tundra, The Cryosphere, 11, 2089–2109, https://doi.org/10.5194/tc-11-2089-2017, 2017.

Transtrum, M. K. and Sethna, J. P.: Improvements to the Levenberg-Marquardt algorithm for nonlinear least-squares minimization, https://doi.org/10.48550/ARXIV.1201.5885, 2012.

Treharne, R., Rogers, B. M., Gasser, T., MacDonald, E., and Natali, S.: Identifying Barriers to Estimating Carbon Release From Interacting Feedbacks in a Warming Arctic, Front. Clim., 3, 716464, https://doi.org/10.3389/fclim.2021.716464, 2022.

Turetsky, M. R., Abbott, B. W., Jones, M. C., Anthony, K. W., Olefeldt, D., Schuur, E. A. G., Grosse, G., Kuhry, P., Hugelius, G., Koven, C., Lawrence, D. M., Gibson, C., Sannel, A. B. K., and McGuire, A. D.: Carbon release through abrupt permafrost thaw, Nat. Geosci., 13, 138–143, https://doi.org/10.1038/s41561-019-0526-0, 2020.

Vesselinov V.V.: MADS: Model Analysis and Decision Support in Julia, https://github.com/madsjulia/Mads.jl, 2022.

Virkkala, A.-M., Abdi, A. M., Luoto, M., and Metcalfe, D. B.: Identifying multidisciplinary research gaps across Arctic terrestrial gradients, Environ. Res. Lett., 14, 124061, https://doi.org/10.1088/1748-9326/ab4291, 2019.

834 Wutzler, T. and Carvalhais, N.: Balancing multiple constraints in model-data integration: Weights and the parameter block
835 approach, JGR Biogeosciences, 119, 2112–2129, https://doi.org/10.1002/2014JG002650, 2014.

836 Xu, T., Valocchi, A. J., Ye, M., Liang, F., and Lin, Y.: Bayesian calibration of groundwater models with input data uncertainty,
837 Water Resources Research, 53, 3224–3245, https://doi.org/10.1002/2016WR019512, 2017.

838 Yi, S., McGuire, A. D., Harden, J., Kasischke, E., Manies, K., Hinzman, L., Liljedahl, A., Randerson, J., Liu, H., Romanovsky,
839 V., Marchenko, S., and Kim, Y.: Interactions between soil thermal and hydrological dynamics in the response of Alaska
840 ecosystems to fire disturbance: SOIL THERMAL AND HYDROLOGICAL DYNAMICS, J. Geophys. Res., 114, n/a-n/a,
841 https://doi.org/10.1029/2008JG000841, 2009.

842 Yi, S., McGuire, A. D., Kasischke, E., Harden, J., Manies, K., Mack, M., and Turetsky, M.: A dynamic organic soil
843 biogeochemical model for simulating the effects of wildfire on soil environmental conditions and carbon dynamics of black
844 spruce forests, J. Geophys. Res., 115, G04015, https://doi.org/10.1029/2010JG001302, 2010.

845 Zhuang, Q., McGuire, A. D., O'Neill, K. P., Harden, J. W., Romanovsky, V. E., and Yarie, J.: Modeling soil thermal and
846 carbon dynamics of a fire chronosequence in interior Alaska, J. Geophys. Res., 108, 8147,
847 https://doi.org/10.1029/2001JD001244, 2002.

848